ACCOUNTS of chemical research

Article

Cite This: Acc. Chem. Res. XXXX, XXX, XXX-XXX

pubs.acs.org/accounts

A Mechanism for Symmetry Breaking and Shape Control in Single-Crystal Gold Nanorods

Michael J. Walsh,*[,†] Wenming Tong,[‡] Hadas Katz-Boon,[†] Paul Mulvaney,[∥] Joanne Etheridge,[†,§] and Alison M. Funston[‡]

[†]Department of Materials Engineering, [‡]ARC Centre of Excellence in Exciton Science and School of Chemistry, and [§]Monash Centre for Electron Microscopy, Monash University, Clayton, Victoria 3800, Australia

[∥]ARC Centre of Excellence in Exciton Science, School of Chemistry, and Bio21 Institute, University of Melbourne, Parkville, Victoria 3010, Australia

CONSPECTUS: The phenomenon of symmetry breaking—in which the order of symmetry of a system is reduced despite manifest higher-order symmetry in the underlying fundamental laws—is pervasive throughout science and nature, playing a critical role in fields ranging from particle physics and quantum theory to cosmology and general relativity. For the growth of crystals, symmetry breaking is the crucial step required to generate a macroscopic shape that has fewer symmetry elements than the unit cell and/or seed crystal from which it grew. Advances in colloid synthesis have enabled a wide variety of nanocrystal morphologies to be achieved, albeit empirically. Of the various nanoparticle morphologies synthesized, gold nanorods have perhaps been the most intensely studied, thanks largely to their unique morphology-dependent optical properties and exciting application potential. However, despite intense research efforts, an understanding of the mechanism by which a single crystal breaks symmetry and grows anisotropically has remained elusive, with many reports presenting seemingly conflicting data and theories. A fundamental understanding of the symmetry breaking process is needed to provide a rational framework upon which future synthetic approaches can be built.

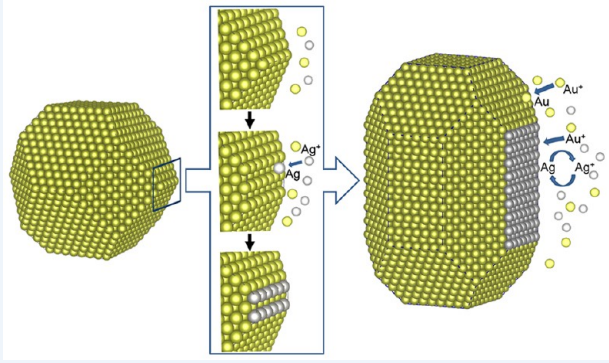

Inspired by recent experimental results and drawing upon the wider literature, we present a mechanism for gold nanorod growth from the moments prior to symmetry breaking to the final product. In particular, we describe the steps by which a cuboctahedral seed particle breaks symmetry and undergoes anisotropic growth to form a nanorod. With an emphasis on the evolving crystal structure, we highlight the key geometrical and chemical drivers behind the symmetry breaking process and factors that govern the formation and growth of nanorods, including control over the crystal width, length, and surface faceting.

We propose that symmetry breaking is induced by an initial formation of a new surface structure that is stabilized by the deposition of silver, thus preserving this facet in the embryonic nanorod. These new surfaces initially form stochastically as truncations that remove high-energy edge atoms at the intersection of existing {111} facets and represent the beginnings of a {011}-type surface. Crucially, the finely tuned $[HAuCl_4]$:$[AgNO_3]$ ratio and reduction potential of the system mean that silver deposition can occur on the more atomically open surface but not on the pre-existing lower-index facets. The stabilized surfaces develop into side facets of the nascent nanorod, while the largely unpassivated {111} facets are the predominant site of Au atom deposition. Growth in the width direction is tightly controlled by a self-sustaining cycle of galvanic replacement and silver deposition. It is the $[HAuCl_4]$:$[AgNO_3]$ ratio that directly determines the particle size at which the more open atomic surfaces can be stabilized by silver and the rate of growth in the width direction following symmetry breaking, thus explaining the known aspect ratio control with Ag ion concentration. We describe the evolving surface faceting of the nanorod and the emergence of higher-index facets. Collectively, these observations allow us to identify facet-size and edge-atom effects as a simple fundamental driver of symmetry breaking and the subsequent development of new surfaces in the presence of adsorbates.

■ INTRODUCTION

Recent advances in colloidal techniques have enabled the synthesis of novel nanoparticle morphologies that exhibit new properties. The unique structure−property relationships of such nanoparticles are perhaps best exemplified by gold nanorods. The anisotropic nanorod shape splits the localized surface plasmon resonance (LSPR) into transverse and longitudinal modes, with the wavelength of the latter directly determined by the particle aspect ratio. This allows the plasmonic properties of gold nanorods[1] to be tailored to specific applications, offering exciting potential for drug delivery

Received: June 22, 2017

DOI: 10.1021/acs.accounts.7b00313
Acc. Chem. Res. XXXX, XXX, XXX−XXX

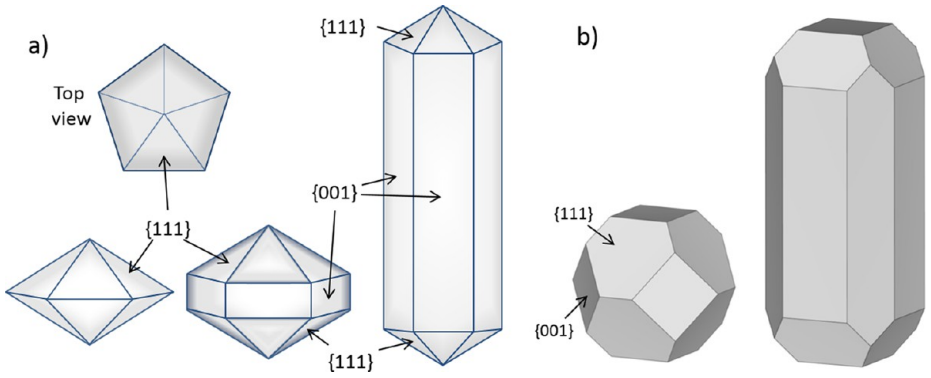

Figure 1. Schematic figures of (a) penta-twinned decahedral and truncated decahedral seed particles and the resultant penta-twinned nanorod and (b) a single-crystal cuboctahedral seed and the resultant single-crystal nanorod.

and "theranostics",[2] while the formation of high-index surface facets is of great interest for heterogeneous catalysis.[3]

However, nanoparticle syntheses have largely been derived empirically,[4,5] with limited understanding of the underpinning growth mechanisms. In single-crystal cases, to generate a particle shape with a lower symmetry number than its precursor requires growth to occur anisotropically along symmetry-equivalent crystal axes, that is, along directions within the unit cell for which the atomic structure is identical. The mechanism(s) by which this symmetry breaking process(es) occurs is the subject of considerable debate. In this Account, we consider this question in the context of the archetypal system of single-crystal gold nanorods, exploring each aspect of the growth mechanism from the initial symmetry breaking event to subsequent anisotropic growth and shape control.

We define "anisotropic shapes" as morphologies that contain facets that are nominally symmetry-equivalent (i.e., facets of the same {*hkl*} family) but differ in their size and/or distance from the particle center. Such morphologies may result from several potential anisotropic growth processes, including growth conditions that cause a limited supply of precursor atoms, asymmetric oxidative etching, particle coalescence, defect formation, and asymmetric surface passivation (see, e.g., ref 6 and references therein). In addition, size effects inherent to small nanoparticle systems may play an important and often overlooked role in crystal growth. These size effects are driven by the significant contribution of edge and corner atoms for small surface facets, meaning that the surface energetics and resulting growth rates will depend critically on facet size and shape in addition to crystallographic orientation.

In the case of single-crystal gold nanorods, the process of selective surface passivation is often proposed to induce anisotropic nanorod growth.[7,8] However, in the absence of twinning, the formation of anisotropic shapes cannot be explained solely by selective surface passivation.[5] For a single-crystal particle with cubic atomic structure ($Fm\bar{3}m$) and octahedral symmetry (O_h), there is no inherent driving force to induce anisotropic growth in symmetry-equivalent directions. For example, in the case of cuboctahedra comprising {111} and {001} facets, selectively stabilizing one facet type at the expense of another will simply produce octahedra or cubes, respectively. Nevertheless, single-crystalline nanorods grow along the ⟨100⟩ axis, with the growth rate in the ⟨100⟩ direction being much greater than those in the ⟨010⟩ and ⟨001⟩ directions even though the atomic structure is identical in all three directions. As such, we must understand how and why growth occurs at different rates along seemingly symmetry-equivalent directions. Clearly, a symmetry breaking event—in which one or more symmetry elements of the seed particle are removed—is needed.

Gold nanorods are typically synthesized through a seed-mediated approach, wherein seed particles are placed into a growth solution containing gold ions, a surfactant such as cetyltrimethylammonium bromide (CTAB), and a weak reducing agent such as ascorbic acid.[9,10] Ascorbic acid reduces Au^{3+} to Au^{+} but importantly not to Au^{0}, with this final reduction step occurring epitaxially on the gold seed particle surface.[9] We note that Au ions are strongly bound to CTAB micelles in solution, forming Au−CTA complexes, from which Au atoms must be released prior to deposition on the nanoparticle surface. As the crystallinity of the particle is maintained throughout growth, the crystal structure of the nanorod is determined by the use of either single-crystal(line) or penta-twinned seeds, resulting in single-crystal or penta-twinned nanorods, respectively.[7] However, the formation of single-crystal nanorods is observed to require the addition of silver ions, with the $AgNO_3$ concentration not only responsible for control of the nanorod aspect ratio[10,11] but actually required to lock in symmetry breaking and enable the onset of anisotropic growth.[8]

In contrast to the single-crystal case, penta-twinned nanorods may grow through a more straightforward selective surface passivation mechanism thanks to the geometry inherent in the penta-twinned seed particles. As shown in Figure 1a, decahedral seeds comprise five identical crystal units bound by {111} surface facets. However, sharp atomic edges at the intersection of facets are rarely favorable, and some level of {001} faceting is common, leading to truncated decahedra. Crucially, this establishes a seed structure with {111} "top and bottom" facets and five {001} "side" facets that share a common orthogonality with the resulting [011] growth direction. In the presence of a surfactant that may selectively passivate a given crystallographic family of facets, the distinct arrangement of {111} versus {001} surfaces provides an intrinsic reason for preferential growth in one direction over the other. This is in stark contrast to the crystallographic isotropy of the single-crystal cuboctahedra used as seeds in single-crystal nanorod growth (Figure 1b).

For single crystals, shape anisotropy was initially thought to be induced by a soft-templating effect of the surfactant micelle.[9−11] CTAB is known to form cylindrical micelles at concentrations typically used for nanorod syntheses, and the expected size of the micelle correlates with the size of the seed particle prior to symmetry breaking.[12] However, templating by

DOI: 10.1021/acs.accounts.7b00313
Acc. Chem. Res. XXXX, XXX, XXX−XXX

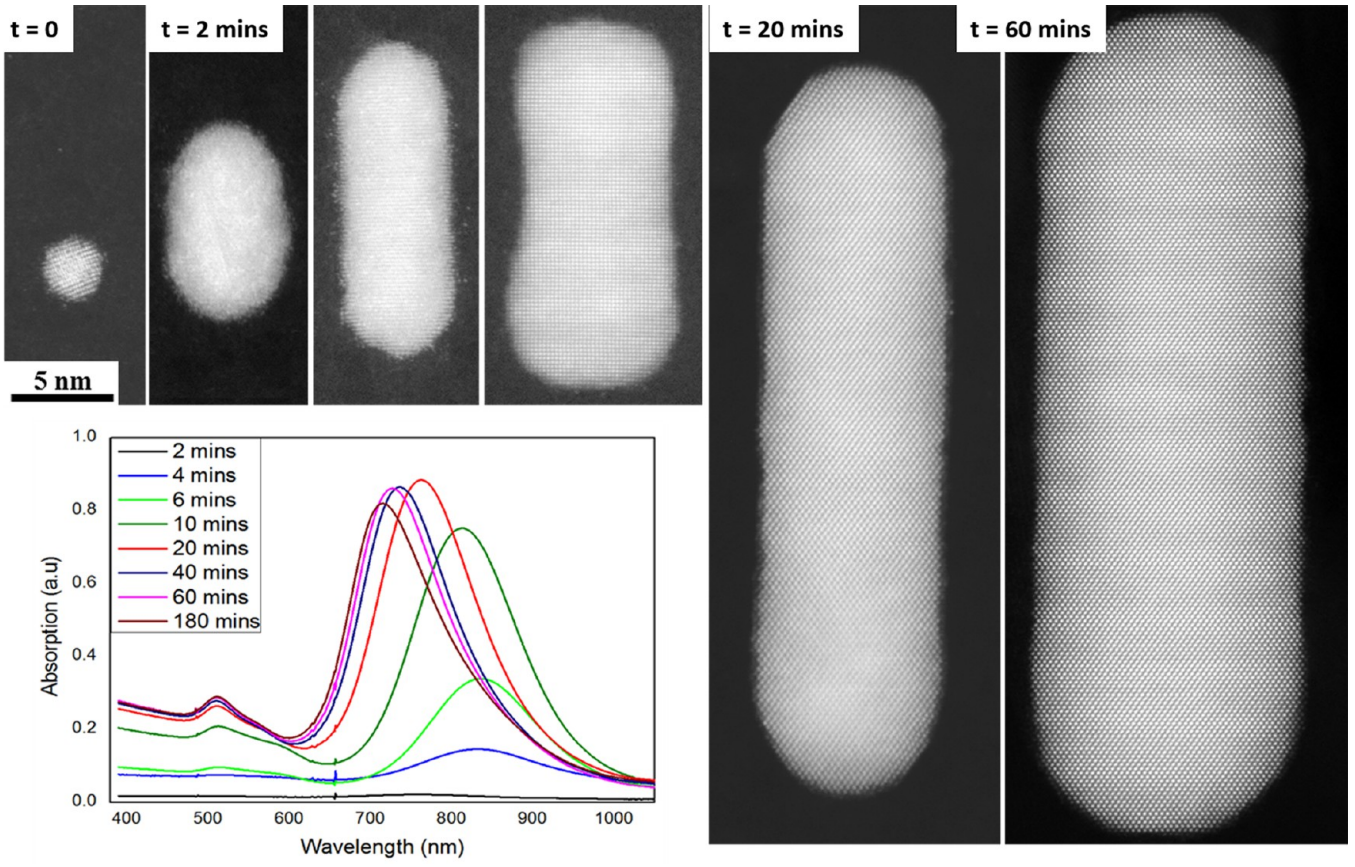

Figure 2. Representative HAADF-STEM images and corresponding UV−vis spectra of gold nanoparticles at various stages of nanorod growth. The methodology is described in ref 8.

CTAB micelles fails to explain the precise control of nanorod dimensions with $AgNO_3$ concentration and the synthesis of various other morphologies under similar conditions. Finally, nanorods can be successfully synthesized below the critical micelle concentration for CTAB with addition of NaBr,[13] and the original choice of CTAB for its micellar structure has since been described as "serendipitous" by Murphy and co-workers.[14] However, halide ions remain a key ingredient in many anisotropic nanoparticle syntheses and can be expected to help control the nanoparticle shape through a variety of mechanisms. These include regulating the redox potential of the metal ions and/or underpotential deposition (UPD) at the nanoparticle surface as well as acting as facet-specific capping agents.[14]

The second major proposed pathway to symmetry breaking and shape anisotropy is selective surface passivation, which can be further broken down into two proposed mechanisms: passivation by AgBr complexes[15,16] and Ag UPD.[7] AgBr complexes have been identified in gold nanorod solutions by several techniques,[15,16] and it has been suggested these complexes are responsible for selectively blocking the side facets of the nanorod, thereby promoting anisotropic growth. However, recent X-ray photoelectron spectroscopy results contradict these earlier reports by showing that the Br^- concentration at the nanoparticle surface is independent of the $[HAuCl_4]$:$[AgNO_3]$ ratio, indicating that a Ag UPD growth mechanism is responsible.[17]

Underpotential deposition is the process by which small amounts of a metal ion may be deposited on a foreign substrate at potentials more positive than those predicted by the Nernst equation. This phenomenon occurs for selected metal couples where the adsorbate interacts more strongly with the substrate material than it does with its own bulk. For example, deposition of submonolayers of silver on gold surfaces can occur at potentials less than those required for bulk deposition of Ag on Au. UPD is driven by the electrochemical potential of the electrons in the redox system and promoted by a larger concentration of metal ions in the growth solution.[18] In addition, bonding effects favor the stabilization of adsorbate layers on higher-index surfaces, as their more open atomic structure provides a stronger attractive potential.[18] Therefore, by careful tuning of the ratio of the metal-ion pair with the redox potential of the system, it is possible to drive UPD on higher-index facets but not others, thereby selectively passivating those surfaces while growth occurs in other directions.[19,20] UPD was originally observed in nanoparticle systems during deposition of Pb on gold nanoparticles[21] and has since become a powerful tool with which one can control the generation of a variety of nanoparticle shapes.[18−20]

In a seminal paper, Liu and Guyot-Sionnest[7] not only showed that the seed structure determines the final crystallinity of the synthesized nanoparticle but also proposed that it is the selective stabilization of {011} side facets by Ag UPD that enables Au nanorod growth. As the reduction potential of the system is approximately 0.3 V, they suggested that a Ag UPD layer may form on {011} side facets but not on other lower-index surfaces. Sanchez and co-workers subsequently calculated the UPD shifts for the Au/Ag^+ system to be 0.12, 0.17, and 0.28 V for Au{111}, Au{001}, and Au{011}, respectively.[22] We note that these potentials were calculated for bulk systems, and the

DOI: 10.1021/acs.accounts.7b00313
Acc. Chem. Res. XXXX, XXX, XXX−XXX

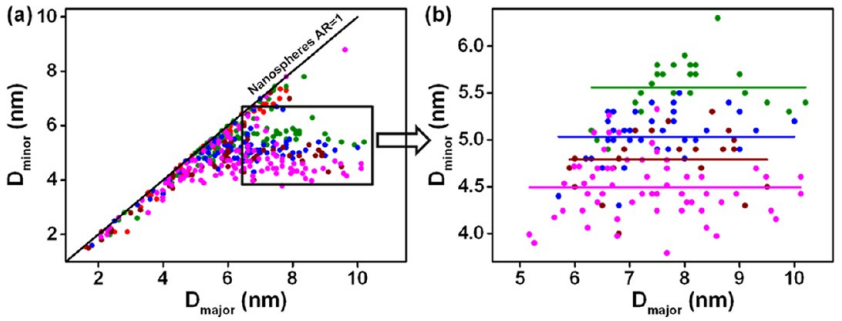

[$AgNO_3$] (μM)	3.2	6.4	9.6	12.7	15.9
Au:$AgNO_3$ (molar)	25	12.5	8.33	6.25	5
Average D_{minor} (nm)	--	5.6 ± 0.3	5.0 ± 0.2	4.8 ± 0.3	4.5 ± 0.3

Figure 3. Size statistics of overgrown seeds with [$HAuCl_4$]:[$AgNO_3$] ratios of 25 (red), 12.5 (olive), 8.33 (blue), 6.25 (wine), and 5 (magenta) using fixed concentrations of gold seeds, CTAB, and ascorbic acid, as described in ref 29. Data are shown for (a) all overgrown seeds and (b) overgrown seeds with aspect ratio ≥ 1.25. Reproduced from ref 29. Copyright 2017 American Chemical Society.

effect of edge atoms must be considered for small facets in nanoparticles.[18] In addition, the effect of surfactants and halides on UPD must be considered for a complete description of relevant nanoparticle growth mechanisms. For example, the presence of anions such as Br^- provides a further attractive interaction with the adsorbate and can be expected to promote the onset of UPD.[23]

Although selective surface passivation—either by Ag UPD or by AgBr complexes—may be a critical part of the process, it would not be expected to differentiate facets with symmetry-equivalent crystallographic indices and hence atomic structure. It therefore cannot explain how a single-crystal particle can grow at different rates on nominally symmetry-equivalent surfaces. To achieve this, the symmetry of the particle must be broken.

In the following sections, we utilize recent experimental results to propose a mechanism for symmetry breaking and gold nanorod growth. With a focus on the growing nanoparticle structure, we break the synthesis into key growth stages and describe the geometrical and chemical drivers that control symmetry breaking, growth in the nanorod length and width directions, and the evolution of surface faceting, which collectively control the growth of single-crystal nanorods.

SINGLE-CRYSTAL GOLD NANOROD GROWTH

Figure 2 shows representative images of gold nanorods at various stages of growth with corresponding UV−vis spectra that describe a sequence of stochastic symmetry breaking, fast anisotropic growth, and finally a slow and approximately isotropic growth phase, in agreement with previous reports.[12,24]

THE SEEDS

As previously highlighted, the structure of the seed particle is crucial for subsequent growth, with seed crystallinity and surface faceting being key determinants of the resulting particle morphology. Typically, a two-step seed-mediated approach is used,[9,10] in which seed particles are synthesized separately (to optimize the monodispersity and yield of the desired size and structure) and then placed into a growth solution. However, one-pot or "seedless" methods also exist, in which seeds are nucleated in the growth solution before catalyzing further growth.[25] A strong reducing agent such as $NaBH_4$ drives rapid nucleation and a close to homogeneous distribution of seed particle sizes. The structure of the seed particles can be determined by the growth kinetics and the addition of surface-passivating surfactants, while the stability of that structure is sensitive to particle size and thermodynamic considerations.[26]

The seeds synthesized in CTAB adopt a single-crystal cuboctahedral morphology bound by a combination of {111} and {001} facets.[7,8] In contrast, gold nanoparticles of a similar size produced using citrate or poly(vinylpyrrolidone) (PVP) surfactants typically adopt multiply twinned structures, such as decahedra, that enable a greater fraction of {111} surfaces to be incorporated. These seeds form crystals with pentagonal cross section, such as penta-twinned nanorods, decahedra, and bipyramids.[4,7,27] The prevalence of cuboctahedra over the thermodynamically expected decahedra and icosahedra again indicates that CTAB reduces the relative surface energy of {001} surfaces, as previously observed in the case of penta-twinned nanorod growth. The seeds synthesized in CTAB for single-crystal nanorod growth have been reported to range in size from nanoclusters to particles up to 4 nm in diameter.[7,8,12,26] Upon introduction to the growth solution, the seeds maintain their cuboctahedral morphology, growing at the same rate in symmetry-equivalent directions, until a critical size is reached,[8,12,28,29] at which point a symmetry breaking event occurs.

SYMMETRY BREAKING

For gold nanorods, both the stochastic nature of the symmetry breaking event and in particular the small sizes at which it occurs has made it challenging to obtain clear experimental evidence as to how a seed particle breaks symmetry.[24] However, recent observations have revealed that symmetry breaking occurs only in the presence of silver and only within a limited size range of 4−7 nm.[8,29] Moreover, the precise size at which particles break symmetry is found to depend directly on the [$HAuCl_4$]:[$AgNO_3$] ratio, with higher silver nitrate concentrations driving symmetry breaking at smaller particle sizes, as shown in Figure 3.[29] Although small, the significant difference in particle size at symmetry breaking as a function of [$HAuCl_4$]:[$AgNO_3$] ratio offers a key clue as to how this event occurs and the crucial role of silver.

Analysis of the atomic structure of the nanocrystals at the symmetry breaking stage enables observation of how the surface faceting and crystal shape develop in the embryonic

DOI: 10.1021/acs.accounts.7b00313
Acc. Chem. Res. XXXX, XXX, XXX−XXX

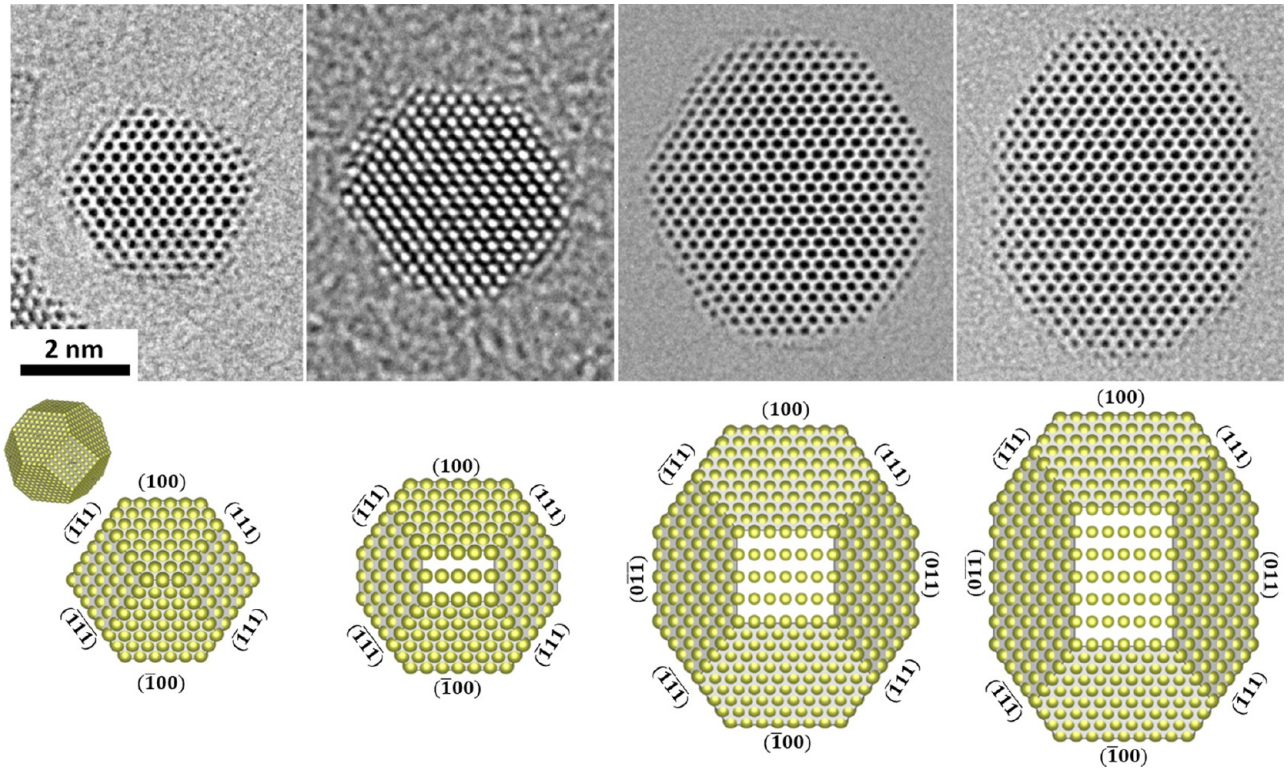

Figure 4. Gold nanocrystals during the symmetry breaking stage of nanorod growth. (top) High-resolution phase-contrast TEM images of particles oriented in the [011] direction. (bottom) Corresponding schematic models. The methodology is described in ref 8.

nanorod.[8,29] Figure 4 shows that at particle diameters as small as approximately 4 nm, truncating surfaces begin to form to remove high-energy edge atoms at the intersection of {111} facets. The initial truncation forms asynchronously and marks the beginnings of a {011}-type surface with a more open atomic structure than the pre-existing {111} and {001} facets. We propose that in the presence of Ag^+ these new surfaces are stabilized and become the elongated "side facets" of the nascent nanorod (Figure 4). Thus, the emergence of new higher-index surfaces marks the key reduction in symmetry of the original seed structure. The effect of the $AgNO_3$ concentration on the size at which this event occurs gives new insights into how the higher-index facets are stabilized.

In extending the phenomenon of UPD to nanoparticle systems, Leiva and co-workers showed that there is an underpotential−overpotential transition that occurs in the limit of small nanoparticles, essentially placing a lower limit on the particle size at which UPD may occur.[30] This can be understood by considering the effect of bonding at corner, edge, and central face atomic sites, with the free energy for adsorption at each collectively determining the surface energy of a given facet. An atom deposited on the central face of a surface facet will be bound to several nearest neighbors, while a deposited edge or corner atom remains highly undercoordinated and as such provides a much greater contribution to the overall new effective surface energy per deposited atom. For a given facet, the number of corner atomic sites is fixed, while the numbers of edge and central face sites grow linearly and quadratically with facet size, respectively, as shown in Figure 5. Therefore, the energy of a given facet per square nanometer increases as the facet size is reduced.[31] This inherent "nanosize effect" requires facet size and shape to be considered important parameters in addition to facet orientation in the limit of small particles.

In the synthesis of gold nanorods, the $AgNO_3$ concentration and redox potential (due primarily to the ascorbate couple) are such that Ag UPD may be expected to occur on {011} and higher-index facets but not the lower-index {111} and {001} surfaces that already exist on the cuboctahedral structure.[7,8] Thus, the emergence of nascent {011} truncations marks the first point at which UPD of Ag may occur, while the atomically rough nature of these emerging facets enhances bonding effects and therefore the expected UPD shift. This process is illustrated schematically in Figure 6.

For small facets, the increased relative contribution of edge and corner atoms means that a stronger driving force (either electric potential or metal ion concentration) is required for Ag UPD to occur. In this context, the observation that the size at which symmetry breaking occurs is determined by the $[HAuCl_4]$:$[AgNO_3]$ ratio[29] may be more fully understood. At the smallest end of the symmetry breaking size range, namely, ∼4 nm, truncating {011} surfaces comprise only a few atoms, with a high proportion of these being edge or corner atoms. The results in Figure 3 show that small truncating {011} surfaces may be stabilized when a sufficiently high concentration of $AgNO_3$ (low $[HAuCl_4]$:$[AgNO_3]$ ratio) is present. However, at lower $AgNO_3$ concentrations, further isotropic particle growth is required until the higher-index {011} surface can be sufficiently large to enable the onset of Ag UPD. We emphasize that it is the $[HAuCl_4]$:$[AgNO_3]$ ratio, rather than simply the $AgNO_3$ concentration, that determines the symmetry breaking size.[29] This important distinction suggests that symmetry breaking may be attributed to a Ag-UPD-dominant process that depends directly on the ratio of gold and silver ions.

DOI: 10.1021/acs.accounts.7b00313
Acc. Chem. Res. XXXX, XXX, XXX−XXX

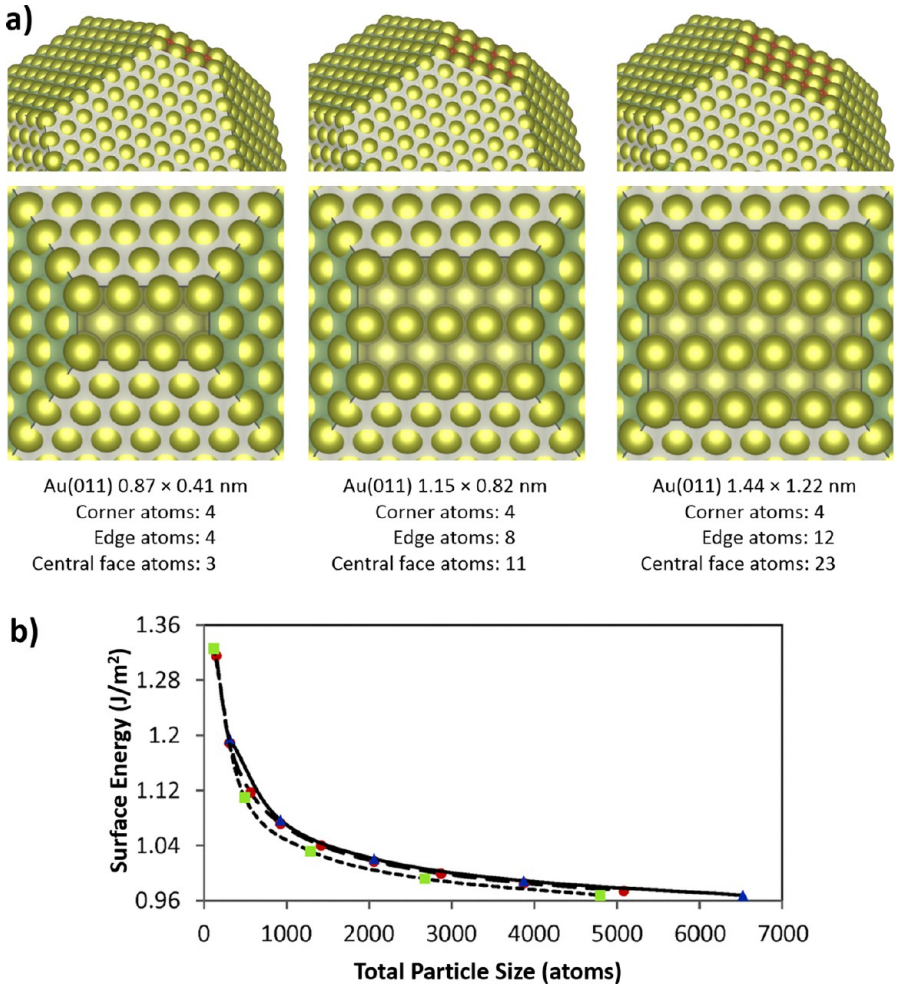

Figure 5. (a) Schematic diagrams of nascent {011} surfaces showing the effect of facet size on the numbers of corner, edge, and central face atomic sites. The particle depicted represents the approximate minimum particle size at which truncating surfaces can form. Below this size, geometrical constraints prevent the removal of edge atoms in favor of a truncating surface. (b) Calculated surface energies for cuboctahedra (blue triangles), truncated octahedra (green squares), and decahedra (red circles) as functions of particle size. Panel (b) is reproduced with permission from ref 31. Copyright 2015 The PCCP Owner Societies.

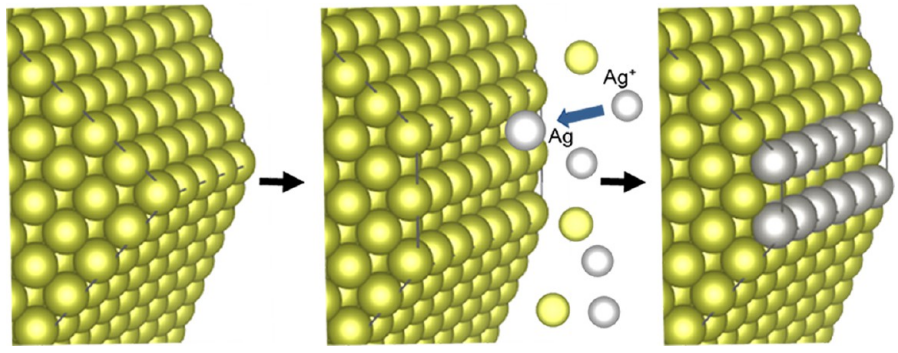

Figure 6. Schematic depiction of the formation of a truncating surface and its stabilization by Ag UPD. The facet size at which Ag deposition can begin is dependent on the $[HAuCl_4]$:$[AgNO_3]$ ratio.

For the upper size limit for symmetry breaking, there comes a point at which further decreasing the $AgNO_3$ concentration no longer provides sufficient driving force to stabilize {011}-type surfaces. This results in a sharp drop in the yield of anisotropic shapes above a symmetry breaking size of approximately 7 nm. The minimum size at which a particle may break symmetry (~4 nm) is fundamentally limited by the smallest size at which the particle can form a {011}-type truncation. At sizes below this, the formation of a truncating surface to remove edge effects is no longer favored, as the original {111} facet comprises only a few atoms and therefore truncation of an edge would involve removal of much of the original facet. The concentration of silver ions required to drive UPD at this minimum size therefore constitutes the maximum $AgNO_3$ concentration that can be used to effectively control the symmetry breaking size.

DOI: 10.1021/acs.accounts.7b00313
Acc. Chem. Res. XXXX, XXX, XXX−XXX

In the following section, we build on these results to show that the connection between the LSPR and the nanorod aspect ratio is effectively determined at the symmetry breaking point and therefore by the parameters that control symmetry breaking.[29] Thus, it is this fundamental limit to the minimum symmetry breaking size that is the origin of the maximum LSPR wavelength that can be achieved by tuning the silver nitrate concentration.

In summary, we propose that the formation of higher-index truncating surfaces marks the key reduction in symmetry of the particle and enables the onset of Ag UPD. The dynamic nature and slow kinetics of growth make this symmetry breaking event stochastic in nature. By stabilization of atomically open {011}-type surfaces, a structure is created in which the surface faceting at the "sides" is distinct from the surfaces at the tips of the nascent rod. Once the emerging side facets are stabilized, a ⟨100⟩ growth direction orthogonal to the new side facets is established, with Au atom deposition taking place predominantly on the unpassivated {111} surfaces. However, we must still understand how, following stabilization of the first truncation, subsequent {011}-type facets form around the "width" of the particle and therefore with a common growth direction. For example, why should the second stabilized surface be $(0\bar{1}1)$ as opposed to (101)? This remains a key unresolved question, and we speculate on possible causes below.

For a perfect cuboctahedron, the formation of a given {011}-type facet is equally likely in any of the 12 equivalent ⟨011⟩ directions. However, the reduction of particle symmetry by the first truncation fundamentally changes several properties of the particle, with each of these having potentially important consequences for the evolving particle structure. First, we have already seen that facet edge and size effects are important considerations in this size range. Creating a new surface clearly alters the symmetry of the facet orientation and edge contributions, while stabilizing that facet and allowing growth on others will cause the elongation of that facet and the edges it influences. Second, the creation of a new surface and the resultant reduction of symmetry of the crystal will change the distribution of mechanical stress. We hypothesize that as a result of the distortion of surface and internal atomic bonds (which are strongly coupled in these tiny particles), the initial truncation will control the location at which a second {011} truncation is formed. The surface tension interlinked with the strong internal mechanical forces in the ⟨011⟩ direction (as indicated by the significant ⟨011⟩ low-frequency transverse acoustic phonon mode in bulk gold) is likely to induce the formation of the second, "paired" {011} truncation and so on, ultimately ensuring the preferential formation of the other three {011} side facets that enable a common growth direction.

Finally, the important role of the CTAB surfactant must be more fully considered. Anionic gold (and silver) complexes will be strongly bound to the CTAB micelles, sequestering those metal ions and reducing the number of Au^+ ions available for growth, thereby providing control over the nanoparticle growth rate.[4] Furthermore, the CTA^+ bilayer stabilizes the particles and reduces the accessibility of ions to the nanoparticle surface, providing further control over the rate of Au deposition. This control of the growth kinetics may enable the original truncation to define the first side facet and resulting nanorod growth direction. The observation of asymmetric tips at intermediate stages of growth is consistent with this hypothesis, with the formation of additional {110} or {101} facets[32] at the tips that lack a common growth direction with the {011} side facets being neither prohibited nor important in defining the original growth direction.

The bromide counterion of CTAB is also a key component for symmetry breaking and nanorod growth.[13,14] Mirkin and co-workers suggested that Br^- may disrupt the Ag UPD layer, with an appropriate Ag^+ to Br^- ratio allowing the Ag UPD layer to be mobile on the particle surface.[20] If this is the case, one can envisage a "zipping" mechanism at the side facets in which the originally deposited Ag can relocate to newly created {011} sites following growth on the adjacent {111} surface, with the CTAB molecule able to maintain the newly formed side-facet geometry. Alternatively, CTAB may bond with the Ag layer and further stabilize it with a synergistic effect to the original Ag UPD,[33] while the presence of Br^- ions may promote Ag UPD.[23] Furthermore, Ag UPD and/or stabilization by CTAB may occur more easily on {001}- and {010}-type surfaces that are adjacent to the stabilized {011} facet relative to the more distant {100} tips, thereby providing a route to different growth rates on crystallographically equivalent surfaces. Further work is needed to determine the precise role(s) of CTA^+ and Br^- in the process of anisotropic growth and the synergies which exist between halide ions and silver ions for selective surface passivation.

INTERMEDIATE STAGES OF GROWTH

We define intermediate growth here as the stage that immediately follows the establishment of a nascent rod structure with identifiable side facets and continues through the observed rapid elongation in particle length until growth slows and the nanorod is close to reaching its maximum aspect ratio. In the following section, we describe the mechanism by which growth continues following symmetry breaking and how this enables control of the nanorod width, length, and resulting aspect ratio.

Particle size analysis as a function of time revealed that while the particle length increases rapidly, growth in the width direction occurs in a slow, uniform, and controlled manner.[29] Our recent results show that the $[HAuCl_4]$:$[AgNO_3]$ ratio at the symmetry breaking point determines both the size at which symmetry breaking occurs and the following rate of growth in the width direction, which together determine the final width of the nanorod.[29] A higher $AgNO_3$ concentration not only results in smaller particle sizes at symmetry breaking but also a reduced rate of growth in the width direction following symmetry breaking.[29] Remarkably, modifying the $[HAuCl_4]$:$[AgNO_3]$ ratio after the onset of anisotropic growth has little effect on the growth rate.[29] On the basis of these results and continuing from our discussion of Ag UPD stabilizing the side facets of the nascent rod, we describe a mechanism by which growth is closely controlled in the width direction.

The formation of a Ag UPD layer on the side facets of the nascent rod and the presence of excess gold ions in solution creates the conditions for galvanic replacement of the Ag layer by Au^+. However, once removed from the surface by a gold atom, the newly freed Ag^+ ion may be immediately reduced back onto the Au surface, creating a self-sustaining cycle of galvanic replacement and Ag deposition, as described in Figure 7. This process of galvanic replacement and coreduction of Ag at the side facets explains several experimental observations. These include the finding that the presence of Ag is required to stabilize new facets in nascent rods at the onset of anisotropic growth,[7,8,29] yet Ag remains at the nanoparticle surface and is

DOI: 10.1021/acs.accounts.7b00313
Acc. Chem. Res. XXXX, XXX, XXX−XXX

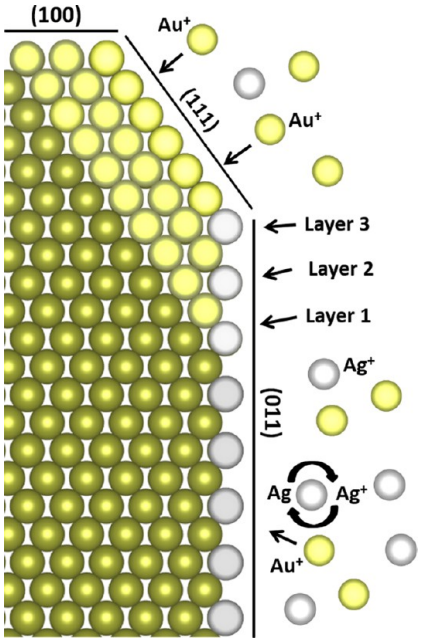

Figure 7. Layer by layer growth on the {111} facet causes the elongation of the side facet by one atom per deposited gold layer. The side facets grow through a slow and self-sustaining cycle of galvanic replacement and silver deposition.

never incorporated into the bulk of the nanoparticle, despite further Au deposition at that surface. In other words, Ag must be replaced at the surface by Au, while submonolayers of Ag are coreduced. Considering an entire side facet, the process of galvanic replacement followed by Ag deposition provides a mechanism for highly controlled layer by layer growth of that facet, with the rate of growth determined by the $[HAuCl_4]$:$[AgNO_3]$ ratio and reduction potential of the system.

In contrast, growth in the nanorod length direction is largely unaffected by the silver concentration[29] and instead seems constrained only by the accessible gold ions for reduction. We propose that gold atom deposition occurs predominantly on relatively unpassivated {111} surfaces, with each deposited {111} layer extending the side facet by one atom, as shown schematically in Figure 7. Under conditions of faster growth, Au atom deposition on {111} surfaces leads to the formation of concave "dumbbells" or "dog bones" as intermediary structures (Figure 8).[8,12,34] As this rapid anisotropic growth phase begins to slow, the concave particles produced undergo a transition to form nanorods with flat and relatively smooth side facets that provide an energetically preferable arrangement of surfactant molecules.[35] The growth mechanism described above explains how the $[HAuCl_4]$:$[AgNO_3]$ ratio directly controls the particle width and how this in turn effectively determines the resultant nanorod length for a given Au^+ concentration, collectively explaining the known control of the nanorod aspect ratio with silver.

FINAL STAGES OF GROWTH

The final stages of nanorod synthesis see an end to rapid anisotropic growth and the onset of a much slower and approximately isotropic growth phase. This results in a gradual increase in particle volume and is often accompanied by a slight blue shift in the longitudinal plasmon resonance due to a small reduction in aspect ratio (Figure 2). Here we focus on the evolution of surface faceting during the intermediate and final

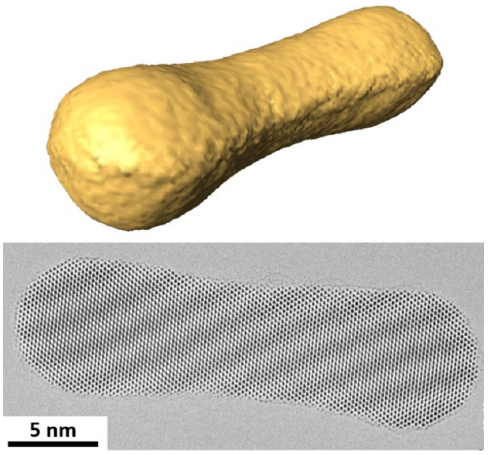

Figure 8. (top) Tomographic reconstruction of ADF-STEM images and (bottom) HRTEM image of a concave gold nanoparticle grown for 6 min in a nanorod growth solution. The methodology is described in refs 8 and 40.

growth stages and the impact this has on the growth kinetics and shape control.

The surface faceting of gold nanorods has been intensely investigated, often with seemingly contradictory results. The faceting generally falls into two categories, those of relatively low index {001} and {011} side facets[32,36] and those of high-index $\{0\ 1\ 1+\sqrt{2}\}$ facets[37] and facets close to this such as {025},[38] while alternating high- and low-index surfaces with comparable surface stability have also been observed.[39] In addition, high-index "bridging" facets that join the side facet with the tip have also been reported.[37,39] It is highly significant that the $\langle 0\ 1\ 1+\sqrt{2}\rangle$ direction perpendicular to the $\{0\ 1\ 1+\sqrt{2}\}$ facet bisects the ⟨001⟩ and ⟨011⟩ directions.[39] In other words, the higher-index $\{0\ 1\ 1+\sqrt{2}\}$ facets truncate the intersection between pre-existing lower-index {001} and {011} facets (Figure 9). This cannot be a coincidence.

We propose the bisecting high-index $\{0\ 1\ 1+\sqrt{2}\}$ facets emerge as truncating or "rounding" surfaces that remove the edge between the existing {001} and {011} side facets. A degree of rounding at facet intersections seems ubiquitous in the reported electron microscopy results of single-crystal gold nanorods.[32,37−39] We hypothesize that earlier-stage rods can be expected to exhibit lower-index surfaces, while more mature rods are likely to have a greater proportion of higher-index facets. A recent study of the evolution of surface faceting for nanorods aged in the original growth solution for 2 h through 13 weeks found that the rods transitioned from being clearly faceted to highly rounded.[40] We note that the effect of the electron beam has been carefully quantified[39] and the experimental conditions carefully chosen to ensure that it is not responsible for the observed changes in nanoparticle morphology.[40] Such rounding of the facets over time is clearly the logical outcome of a truncating mechanism at facet edges.

It is clear that growth time becomes a key factor in the observed morphology, faceting, and surfactant distribution on the nanorods. The described mechanism of facet evolution leads to surface faceting—and therefore the location of silver and surfactants on that surface—at the latter stages of rod growth that are entirely different than for the nascent rods. We therefore propose that the location of silver at the final stages of rod growth is unlikely to be representative of the situation during symmetry breaking and the formation of nascent

DOI: 10.1021/acs.accounts.7b00313
Acc. Chem. Res. XXXX, XXX, XXX−XXX

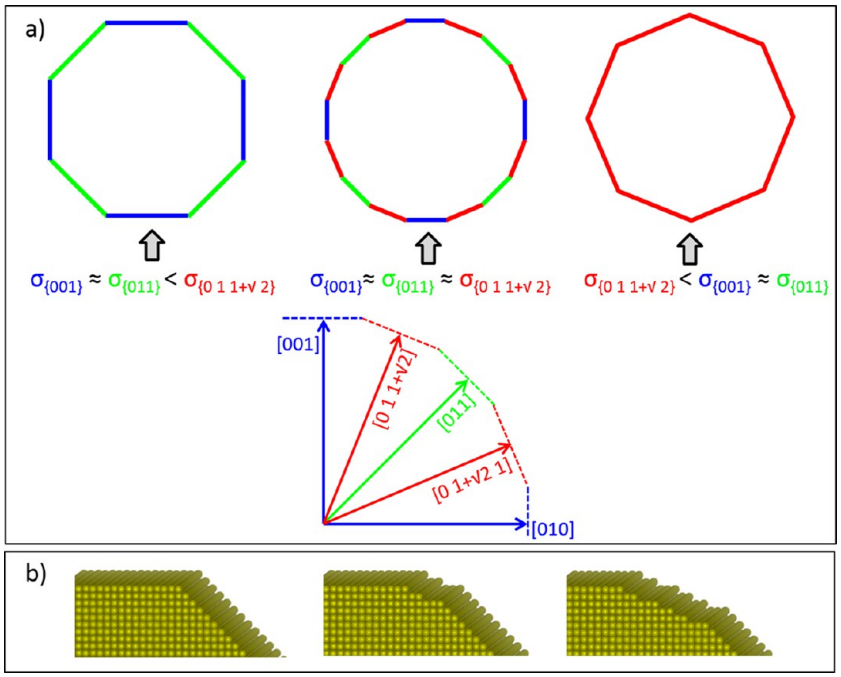

Figure 9. (a) The full gamut of observed (left) low-, (right) high-, and (center) mixed-index side facets are described by the combination of {001}, {011}, and {0 1 1+$\sqrt{2}$} surfaces and their relative surface energies (σ). (b) Atomic models of (left) a sharp atomic edge, (middle) a truncated edge, and (right) a high-index (0 1 1+$\sqrt{2}$) facet at the intersection between low-index (001) and (011) surfaces.

nanorods. Experimentally determining the location of silver at this crucial growth stage, where the nanorods and facets are very small, remains an outstanding challenge.

The development of higher-index surfaces at the bridging or tip facets also has important implications for nanorod growth. A process similar to that for the side facets is observed for the {111} surfaces, leading to the development of {101} and higher-index surfaces and finally rounded tips.[40] The eventual removal of {111} facets ends the arrangement of distinct faceting at the tips relative to the sides and replaces the dominant site for gold atom deposition and growth with a surface capable of being stabilized by silver and CTAB. Therefore, it may be this facet development that ultimately limits the nanorod length by signaling the end of the anisotropic growth phase.

CONCLUSIONS

We have presented a mechanism for gold nanorod growth, describing the process by which the symmetry of the crystal is broken and how the nanorod morphology is determined through control of the crystal width, length, and surface faceting. Electron microscopy observations reveal the emergence of higher-index truncating surfaces that reduce the symmetry of the crystal and enable the onset of Ag UPD. The particle size limits within which this process can occur are fundamentally constrained by a combination of geometrical and chemical factors. Collectively, these constraints explain the aspect ratio control of gold nanorods by silver and in turn confine the resonant surface plasmon wavelengths that can be tuned by this mechanism. For small particles in the presence of adsorbates, the effect of facet edge atoms and their mitigation by the formation of new truncating surfaces emerges as a simple fundamental driver of the reduction of symmetry of the nanocrystal as well as the development of new higher-index surfaces. We expect that a mechanistic understanding of symmetry breaking and shape control will provide a rational basis upon which future anisotropic syntheses can be built.

AUTHOR INFORMATION

Corresponding Author

*E-mail: michael.j.walsh@monash.edu.

ORCID

Michael J. Walsh: 0000-0002-6591-0772
Wenming Tong: 0000-0002-4831-4960
Paul Mulvaney: 0000-0002-8007-3247
Joanne Etheridge: 0000-0002-3199-3936
Alison M. Funston: 0000-0002-4320-6434

Notes

The authors declare no competing financial interest.

Biographies

Dr. Michael J. Walsh is a research fellow in the Department of Materials Science and Engineering at Monash University, Melbourne, Australia. He received his B.Sc. in Physics in 2008 and his Ph.D in 2013 from the University of York, U.K., working under the supervision of Prof. Ed Boyes and Prof. Pratibha Gai. His research focuses on the growth mechanisms, structure−property relationships, and catalytic properties of metal nanoparticles.

Dr. Wenming Tong obtained his B.Sc. in Applied Chemistry in 2003 and his M.Sc. in Chemistry in 2010 at Inner Mongolia University, China. He completed his Ph.D. in 2017 at Monash University under the supervision of Dr. Alison Funston and Prof. Joanne Etheridge. His research interests include the growth and optical properties, including single-particle spectroscopy, of metal nanoparticles.

Dr. Hadas Katz-Boon received her B.Sc. in Material Engineering and B.A in Chemistry in 2002 and her M.B.A. in 2006 from Technion − Israel Institute of Technology, Haifa, Israel. She worked as a metallurgist in the Materials and Process Department in the Israeli

DOI: 10.1021/acs.accounts.7b00313
Acc. Chem. Res. XXXX, XXX, XXX−XXX

Air Force from 2002 to 2006 before moving to Monash University, Australia, where she received her Ph.D. in 2010 under the supervision of Prof. Joanne Etheridge. In 2010 she joined the Materials Science and Engineering Department at Monash University as a research fellow. Her research focuses on developing advanced quantitative scanning transmission electron microscopy methods to examine the 3D shapes of nanoparticles and their surface crystallography.

Prof. Paul Mulvaney is the Director of the new ARC Centre of Excellence in Excition Science and Professor of Chemistry in the School of Chemistry and Bio21 Institute at the University of Melbourne. He was a recent ARC Laureate Fellow from 2011 to 2015 and an ARC Federation Fellow from 2006 to 2010.

Prof. Joanne Etheridge is the Director of the Monash Centre for Electron Microscopy and Professor in the Department of Materials Science and Engineering at Monash University. She obtained her Bachelor's degree and Ph.D. in physics at the University of Melbourne and RMIT University, respectively. She then held appointments at the University of Cambridge Department of Materials Science and Metallurgy, including a Royal Society University Research Fellowship. She returned to Melbourne to join Monash University, where she established the Monash Centre for Electron Microscopy. She conducts research in the theory and development of electron scattering methods for determining the atomic and electronic structure of condensed matter. She also applies these methods to the study of structure–property relationships in functional materials, including nanoparticle and perovskite systems.

Dr. Alison M. Funston is a lecturer in the School of Chemistry at Monash University, Melbourne, Australia. She received her Ph.D. from The University of Melbourne, Australia, in 2002, followed by postdoctoral appointments from 2002 to 2005 at Brookhaven National Laboratory (with Dr. John Miller) and 2006 to 2010 at The University of Melbourne (with Prof. Paul Mulvaney). She moved to Monash as a lecturer in 2010 and was an ARC Future Fellow in 2011–2015. Her research focuses on the synthesis, assembly, and spectroscopy of nanoscale systems, including energy transport and optical properties of well-defined assemblies of metal and semiconductor nanocrystals.

■ ACKNOWLEDGMENTS

This work was supported by Australian Research Council (ARC) Grants DP120101573, DP160104679, and CE170100026 and used microscopes at the Monash Centre for Electron Microscopy funded by ARC Grants LE0454166 and LE100100227. W.T. thanks the Australian Department of Education and Training and Monash University for IPRS and APA scholarships. A.M.F. acknowledges support from the ARC through Future Fellowship funding (FT110100545). P.M. thanks the ARC for support under Grant LF100100117.

■ REFERENCES

(1) Pérez-Juste, J.; Pastoriza-Santos, I.; Liz-Marzán, L. M.; Mulvaney, P. Gold nanorods: Synthesis, characterization and applications. *Coord. Chem. Rev.* **2005**, *249*, 1870–1901.

(2) Dreaden, E. C.; Alkilany, A. M.; Huang, X.; Murphy, C. J.; El-Sayed, M. A. The golden age: gold nanoparticles for biomedicine. *Chem. Soc. Rev.* **2012**, *41*, 2740–2779.

(3) Zhou, Z.-Y.; Tian, N.; Li, J.-T.; Broadwell, I.; Sun, S.-G. Nanomaterials of high surface energy with exceptional properties in catalysis and energy storage. *Chem. Soc. Rev.* **2011**, *40*, 4167–4185.

(4) Grzelczak, M.; Perez-Juste, J.; Mulvaney, P.; Liz-Marzan, L. M. Shape control in gold nanoparticle synthesis. *Chem. Soc. Rev.* **2008**, *37*, 1783–1791.

(5) Lofton, C.; Sigmund, W. Mechanisms Controlling Crystal Habits of Gold and Silver Colloids. *Adv. Funct. Mater.* **2005**, *15* (7), 1197–1208.

(6) Gilroy, K. D.; Peng, H. C.; Yang, X.; Ruditskiy, A.; Xia, Y. Symmetry breaking during nanocrystal growth. *Chem. Commun.* **2017**, *53*, 4530–4541.

(7) Liu, M.; Guyot-Sionnest, P. Mechanism of Silver(I)-Assisted Growth of Gold Nanorods and Bipyramids. *J. Phys. Chem. B* **2005**, *109*, 22192–22200.

(8) Walsh, M. J.; Barrow, S. J.; Tong, W.; Funston, A. M.; Etheridge, J. Symmetry Breaking and Silver in Gold Nanorod Growth. *ACS Nano* **2015**, *9*, 715–724.

(9) Jana, N. R.; Gearheart, L.; Murphy, C. J. Seed-Mediated Growth Approach for Shape-Controlled Synthesis of Spheroidal and Rod-like Gold Nanoparticles Using a Surfactant Template. *Adv. Mater.* **2001**, *13*, 1389–1393.

(10) Nikoobakht, B.; El-Sayed, M. A. Preparation and Growth Mechanism of Gold Nanorods (NRs) Using Seed-Mediated Growth Method. *Chem. Mater.* **2003**, *15*, 1957–1962.

(11) Yu, Y.-Y.; Chang, S.-S.; Lee, C.-L.; Wang, C. R. C Gold Nanorods: Electrochemical Synthesis and Optical Properties. *J. Phys. Chem. B* **1997**, *101*, 6661–6664.

(12) Park, K.; Drummy, L. F.; Wadams, R. C.; Koerner, H.; Nepal, D.; Fabris, L.; Vaia, R. A. Growth Mechanism of Gold Nanorods. *Chem. Mater.* **2013**, *25*, 555–563.

(13) Garg, N.; Scholl, C.; Mohanty, A.; Jin, R. The Role of Bromide Ions in Seeding Growth of Au Nanorods. *Langmuir* **2010**, *26*, 10271–10276.

(14) Lohse, S. E.; Burrows, N. D.; Scarabelli, L.; Liz-Marzán, L. M.; Murphy, C. J. Anisotropic Noble Metal Nanocrystal Growth: The Role of Halides. *Chem. Mater.* **2014**, *26*, 34–43.

(15) Hubert, F.; Testard, F.; Spalla, O. Cetyltrimethylammonium Bromide Silver Bromide Complex as the Capping Agent of Gold Nanorods. *Langmuir* **2008**, *24*, 9219–9222.

(16) Niidome, Y.; Nakamura, Y.; Honda, K.; Akiyama, Y.; Nishioka, K.; Kawasaki, H.; Nakashima, N. Characterization of silver ions adsorbed on gold nanorods: surface analysis by using surface-assisted laser desorption/ionization time-of-flight mass spectrometry. *Chem. Commun.* **2009**, *0*, 1754–1756.

(17) Zhang, Q.; Jing, H.; Li, G. G.; Lin, Y.; Blom, D. A.; Wang, H. Intertwining Roles of Silver Ions, Surfactants, and Reducing Agents in Gold Nanorod Overgrowth: Pathway Switch between Silver Underpotential Deposition and Gold–Silver Codeposition. *Chem. Mater.* **2016**, *28*, 2728–2741.

(18) Mariscal, M. M.; Oviedo, O. A.; Leiva, E. P. M. On the selective decoration of facets in metallic nanoparticles. *J. Mater. Res.* **2012**, *27*, 1777–1786.

(19) Personick, M. L.; Langille, M. R.; Zhang, J.; Mirkin, C. A. Shape Control of Gold Nanoparticles by Silver Underpotential Deposition. *Nano Lett.* **2011**, *11* (8), 3394–3398.

(20) Langille, M. R.; Personick, M. L.; Zhang, J.; Mirkin, C. A. Defining Rules for the Shape Evolution of Gold Nanoparticles. *J. Am. Chem. Soc.* **2012**, *134*, 14542–14554.

(21) Mulvaney, P.; Giersig, M.; Henglein, A. Surface Chemistry of Colloidal Gold: Deposition of Lead and Accompanying Optical Effects. *J. Phys. Chem.* **1992**, *96*, 10419–10424.

(22) Rojas, M. I.; Sanchez, C. G.; Del Pópolo, M. G.; Leiva, E. P. M. Erratum to: "An embedded atom approach to underpotential deposition phenomena": [Surf. Sci. **999**. 421, 59]. *Surf. Sci.* **2000**, *453*, 225–228.

(23) Giménez, M. C.; Ramirez-Pastor, A. J.; Leiva, E. P. M. A model for underpotential deposition in the presence of anions. *J. Chem. Phys.* **2010**, *132*, 184703.

(24) Edgar, J. A.; McDonagh, A. M.; Cortie, M. B. Formation of Gold Nanorods by a Stochastic "Popcorn" Mechanism. *ACS Nano* **2012**, *6*, 1116–1125.

(25) Straney, P. J.; Andolina, C. M.; Millstone, J. E. Seedless Initiation as an Efficient, Sustainable Route to Anisotropic Gold Nanoparticles. *Langmuir* **2013**, *29*, 4396–4403.

DOI: 10.1021/acs.accounts.7b00313
Acc. Chem. Res. XXXX, XXX, XXX–XXX

(26) Park, K.; Hsiao, M.-S.; Koerner, H.; Jawaid, A.; Che, J.; Vaia, R. A. Optimizing Seed Aging for Single Crystal Gold Nanorod Growth: The Critical Role of Gold Nanocluster Crystal Structure. *J. Phys. Chem. C* **2016**, *120*, 28235−45.
(27) Sánchez-Iglesias, A.; Winckelmans, N.; Altantzis, T.; Bals, S.; Grzelczak, M.; Liz-Marzán, L. M. High-Yield Seeded Growth of Monodisperse Pentatwinned Gold Nanoparticles through Thermally Induced Seed Twinning. *J. Am. Chem. Soc.* **2017**, *139*, 107−110.
(28) Hubert, F.; Testard, F.; Rizza, G.; Spalla, O. Nanorods versus Nanospheres: A Bifurcation Mechanism Revealed by Principal Component TEM Analysis. *Langmuir* **2010**, *26*, 6887−6891.
(29) Tong, W.; Walsh, M. J.; Mulvaney, P.; Etheridge, J.; Funston, A. M. Control of Symmetry Breaking Size and Aspect Ratio in Gold Nanorods: the Underlying Role of Silver Nitrate. *J. Phys. Chem. C* **2017**, *121*, 3549−3559.
(30) Oviedo, O. A.; Reinaudi, L.; Leiva, E. P. M. The limits of underpotential deposition in the nanoscale. *Electrochem. Commun.* **2012**, *21*, 14−17.
(31) Ali, S.; Myasnichenko, V. S.; Neyts, E. C. Size-dependent strain and surface energies of gold nanoclusters. *Phys. Chem. Chem. Phys.* **2016**, *18*, 792−800.
(32) Goris, B.; Bals, S.; Van den Broek, W.; Carbó-Argibay, E.; Gómez-Graña, S.; Liz-Marzán, L. M.; Van Tendeloo, G. Atomic-scale determination of surface facets in gold nanorods. *Nat. Mater.* **2012**, *11*, 930−935.
(33) Meena, S. K.; Sulpizi, M. From Gold Nanoseeds to Nanorods: The Microscopic Origin of the Anisotropic Growth. *Angew. Chem.* **2016**, *128*, 12139−12143.
(34) Gou, L.; Murphy, C. J. Fine-Tuning the Shape of Gold Nanorods. *Chem. Mater.* **2005**, *17*, 3668−3672.
(35) Grochola, G.; Snook, I. K.; Russo, S. P. Computational modeling of nanorod growth. *J. Chem. Phys.* **2007**, *127*, 194707.
(36) Wang, Z. L.; Mohamed, M. B.; Link, S.; El-Sayed, M. A. Crystallographic facets and shapes of gold nanorods of different aspect ratios. *Surf. Sci.* **1999**, *440*, L809−L814.
(37) Katz-Boon, H.; Rossouw, C.; Weyland, M.; Funston, A. M.; Mulvaney, P.; Etheridge, J. Three-Dimensional Morphology and Crystallography of Gold Nanorods. *Nano Lett.* **2011**, *11*, 273−278.
(38) Carbó-Argibay, E.; Rodríguez-González, B.; Gómez-Graña, S.; Guerrero-Martínez, A.; Pastoriza-Santos, I.; Pérez-Juste, J.; Liz-Marzán, L. M. The Crystalline Structure of Gold Nanorods Revisited: Evidence for Higher-Index Lateral Facets. *Angew. Chem., Int. Ed.* **2010**, *49*, 9397−9400.
(39) Katz-Boon, H.; Walsh, M. J.; Dwyer, C.; Mulvaney, P.; Funston, A. M.; Etheridge, J. Stability of Crystal Facets in Gold Nanorods. *Nano Lett.* **2015**, *15*, 1635−1641.
(40) Tong, W.; Katz-Boon, H.; Walsh, M. J.; Etheridge, J.; Funston, A. M. The Evolution of Size, Shape, and Surface Morphology of Gold Nanorods. Manuscript in preparation.

DOI: 10.1021/acs.accounts.7b00313
Acc. Chem. Res. XXXX, XXX, XXX−XXX